1-1-2009

Bauschinger effect in Nb and V alloyed line-pipe steels

Andrii Kostryzhev
University of Birmingham, andrii@uow.edu.au

Martin Strangwood
University of Birmingham

Claire L. Davis
University of Birmingham

Bauschinger effect in Nb and V alloyed line-pipe steels

Abstract

The UOE process is used for cold forming of large diameter steel line-pipes. Pipe strength has been found to increase (work hardening) or decrease (Bauschinger effect) after the UOE process compared to the plate depending on the steel grade, plate and pipe processing history. The steel chemistry, through the presence of microalloy precipitates, and prior processing, through the size and distribution of microalloy precipitates and presence of retained work hardening, affects the magnitude of the Bauschinger effect. In this paper the microstructures of two (Nb and Nb-V alloyed) steel plates, in terms of (Nb,V)(C,N) particle distributions and dislocation densities, have been related to the Bauschinger parameters in the as rolled and annealed initial conditions. The Bauschinger stress parameter increases with microalloy particle number density and dislocation density increase and the relative importance of the two effects is discussed.

Keywords

bauschinger, effect, steels, pipe, nb, line, alloyed, v

Disciplines

Engineering | Science and Technology Studies

Publication Details

Kostryzhev, A. G., Strangwood, M. & Davis, C. L. (2009). Bauschinger effect in Nb and V alloyed line-pipe steels. Ironmaking and Steelmaking, 36 (3), 186-192.

BAUSCHINGER EFFECT IN Nb- AND V-ALLOYED LINE-PIPE STEELS

A. G. Kostryzhev, M. Strangwood, and C. L. Davis
Department of Metallurgy and Materials, University of Birmingham,
Edgbaston, Birmingham, B15 2TT

ABSTRACT

The UOE process is used for cold forming of large diameter steel line-pipes. Pipe strength has been found to increase (work hardening) or decrease (Bauschinger effect) after the UOE process compared to the plate depending on the steel grade, plate and pipe processing history. The steel chemistry, through the presence of microalloy precipitates, and prior processing, through the size and distribution of microalloy precipitates and presence of retained work hardening, affects the magnitude of the Bauschinger effect. In this paper the microstructures of two (Nb- and Nb-V-alloyed) steel plates, in terms of (Nb,V)(C,N) particle distributions and dislocation densities, have been related to the Bauschinger parameters in the as-rolled and annealed initial conditions. The Bauschinger stress parameter increases with microalloy particle number density and dislocation density increase and the relative importance of the two effects is discussed.

Keywords: Linepipe steels, Bauschinger effect, Work hardening, Microalloyed steels, UOE forming, Precipitation

INTRODUCTION

Transverse mechanical properties of large diameter (> 400 mm) welded steel pipes for the oil and gas industry depend on the thermo-mechanically controlled rolled (TMCR) plate microstructure and the UOE forming process deformation sequence (Figure 1). The TMCR plate microstructure influences the properties via grain refinement, solid solution and precipitation strengthening mechanisms, and retained work-hardening (dislocation substructure). The relative contribution of the strengthening mechanisms depends on the steel composition and rolling process parameters. Cold deformation, for UOE forming typically 1 - 7 % strain range, may result in strength increase (due to further work-hardening) or decrease (due to the Bauschinger effect). Work-hardening during unidirectional deformation (work-softening during reverse deformation) is known to be dependent on the strain level, strain direction and the steel chemistry.

Severe application conditions (low temperature, high internal pressure, corrosive environment) require high strength with simultaneously high toughness for the line-pipe material. Together with the need for good weldability, this has led to decreasing carbon content and increasing microalloying element level in the steel chemistry (Table 1) [1-5]. The combined action of microalloying and TMCR processing results in significant grain refinement and precipitation strengthening. Introduction of accelerated cooling and decreasing finish rolling temperature gives further plate strength increase [6, 7,8].

The Bauschinger effect in line-pipe steels has been previously observed with respect to pipe property test specimen flattening [9]. Mechanical test specimens cut from the 180^0 position to the weld and flattened showed 20% lower yield strength than the pipe ring hydraulic expansion test specimens [1]. Decrease in yield stress from plate to pipe during UOE forming was found to be dependent on the forming conditions, namely the strain level during the different forming stages [10], for example, with an increase in reduction after O-ing up to 1.1% the yield stress decreased by 2% in a 0.106wt%C-0.035Nb-0.035V steel. Recent study of Nb, Nb-V [11] and Mo-Nb-V [12] alloyed steels showed a

dependence of the Bauschinger effect parameters on the chemical composition of the steels and plate processing history. Using the back stress [13] and Orowan [14] theories of the Bauschinger effect it is possible to correlate plate to pipe property change with the dislocation structure (processing history) and microalloying precipitates (steel composition). At the moment Bauschinger parameter dependence on the dislocation structure and the steel chemistry is only known qualitatively. Thus a quantitative dependence of the Bauschinger stress parameter on the precipitate number density and dislocation density is needed. The influence of the microalloy particle volume fraction on the Bauschinger stress parameter was investigated recently using X60 and X65 line-pipe steel examples [15]. In this paper particle number density and dislocation density influence on the Bauschinger stress parameter is presented.

MATERIALS AND EXPERIMENTAL TECHNIQUES

Two different steel plates were provided by Corus plc, Plates and Commercial Steels (Table 2). The C-Nb plates were 10.2 mm in thickness and C-Nb-V 10.5 mm. Mechanical properties meet the requirements of American Petroleum Industry (API) for the grade X60 (C-Nb) and X65 (C-Nb-V) (Table 3). For *optical microscopy and image analysis* sections of approximately 10 mm x 10 mm x 10 mm in size were cut from the as-received plates, mounted in conductive bakelite parallel and perpendicular to the rolling direction, ground and polished to a 1 μm finish then etched in 2% nital. The specimens were imaged using Leica DMRX and Zeiss Axioskop2 microscopes and analysed using KS 300 and KS 400 software. Grain size was measured as average grain diameter for 800-2000 grains and pearlite percent for 5 images at a magnification of 100x (0.161 mm^2) or at a magnification of 200x (0.039 mm^2) depending on the steel grade. Measurements were made across the plate thickness in 0.4 mm steps.

Scanning electron microscopy (SEM) was carried out using a Jeol JSM-7000F field emission gun scanning electron microscope. Nb- and Nb-Ti-rich precipitates were imaged from 4 regions, ferrite and pearlite, sub-surface and mid-thickness, and characterised in terms of size, morphology and area fraction. For the determination of the particle size distributions and area fraction in the C-Nb steel 630 particles from 15585 μm^2 and in the C-Nb-V steel 1064 particles from 10780 μm^2 total area were imaged.

Transmission electron microscopy (TEM) was carried out on Philips-CM20 and Philips Tecnai F20 field emission gun TEMs. V-rich particles in the C-Nb-V steel were imaged from 2 regions, plate mid-thickness and sub-surface. For the determination of the particle size distributions and volume fraction 469 particles from 3.91 μm^2 at sub-surface position and 918 particles from 3.12 μm^2 at mid-thickness position in C-Nb-V as-rolled steel, and 688 particles from 3.35 μm^2 in the C-Nb-V annealed steel at mid-thickness position were imaged. Foil thickness was determined using a convergent beam diffraction technique [16]. Precipitate compositions were determined using *energy dispersive X-ray spectroscopy* (EDS) point analysis in the Jeol-6300 SEM (Noran EDS, Vantage software), Jeol-7000F SEM (Inca Oxford EDS) and Philips-CM20 TEM (Link Oxford EDS). For the Ti-, Nb- and V-rich precipitate chemical composition investigation 54 particles in the C-Nb and 65 particles in the C-Nb-V steel were used. Dislocation sub-structures were studied using Philips-CM20 and Philips Tecnai F20 TEMs. For the dislocation density determination 20 representative regions were imaged in each of the as-rolled and annealed C-Nb and C-Nb-V steels from the plate mid-thickness position. The mid-thickness position was selected to correlate dislocation density with mechanical property data obtained from the compression-tension samples.

Compression-tension testing was carried out on an ESH 250 kN servo-hydraulic twin column low speed ramp universal testing machine. For the stress-strain curve determination 4 cylindrical specimens of 4.5 mm diameter and 13 mm gauge length were cut in the transverse orientation to the rolling direction from the C-Nb and C-Nb-V as-received and annealed steel plates. *Thermodynamic modelling* was carried out using version Q of Thermo-Calc using the bulk alloy composition as an input. Equilibrium phase balances within the temperature range 600-1600 K were calculated along with phase compositions. For ferrite *micro-hardness* distributions across the plate thickness 5 indents for each point were measured using a Shimadzu Vickers micro-hardness tester at intervals of 0.2mm. A load of 500 g was used.

RESULTS

Microstructure characterisation

Optical microscopy of the two steels showed banded ferrite-pearlite microstructures. Sub-surface plate areas showed smaller grain sizes than the mid-thickness. Second phase (pearlite) content increased towards the centre-line consistent with macro-segregation. Average pearlite content decreased with decreasing carbon content in the C-Nb-V steel compared to the C-Nb steel, but the average ferrite micro-hardness increased slightly due to the small amount of grain refinement, precipitation strengthening (from the VC precipitates, discussed later) and work-hardening (determined from TEM and differential scanning calorimetry measurements, presented later), Table 4.

SEM EDS of the >10 nm diameter particles in the C-Nb and C-Nb-V steels revealed these to be Nb-rich and Nb-Ti-rich, which corresponds with Thermo-Calc predictions. Particles of diameter larger than 100 nm exhibited a greater Ti level consistent with precipitation at higher temperatures giving more time for growth, than solely Nb(C,N) which forms at lower temperatures. However, Nb and Nb-Ti containing particle average diameter and area fraction were calculated together. For the number of particles measured in this work, Figure 2, area fraction can be considered equal to the volume fraction and compared with the Thermo-Calc theoretical prediction.

Average particle diameter and volume fraction increase towards the mid-thickness of the plates due to macro-segregation and slower cooling rates during solidification (Table 5), though in the C-Nb-V steel this increase was not significant. Volume fraction in pearlite was larger than that in ferrite due to micro-segregation, consistent with previous studies [17]. Particle volume fraction increases with the increase in microalloying elements from the C-Nb to the C-Nb-V steel as was predicted by Thermo-Calc. The smaller Nb-rich particle diameter observed in the C-Nb-V steel can be explained by the processing variable differences, including lower finish roll temperature for the C-Nb-V steel (735 ^{0}C) than for the C-Nb steel (745 ^{0}C). As SEM measurements do not take into account many fine V-rich precipitates the measured value for the particle volume fraction in the C-Nb-V steel is significantly lower than predicted Thermo-Calc value. Particle number density corresponds to the distribution of the volume fraction, but in the C-Nb-V steel slight decrease in number density towards mid-thickness is observed.

Measured with TEM (Figure 3) the V-rich particle volume fraction increased from f = 0.00069 at the sub-surface to f = 0.00118 at the mid-thickness position due to macro-segregation. Average particle diameter was calculated as 6.3 nm in the mid-thickness and 9.0 nm in the sub-surface areas of the C-Nb-V as-rolled steel. Particle number density was measured as 1578 μm^{-3} at the sub-surface and 3873 μm^{-3} at the mid-thickness position. The decrease in particle diameter and increase in particle number density towards mid-thickness can be partially explained if an increased dislocation density, due to

strain gradients during rolling, gives an increased number density of nucleation sites, but this requires further investigation.

Annealing at 550 ^{0}C for 30 min did not influence the particle distributions in the C-Nb steel (Figure 3,a,b). This corresponds with the reported stability of NbC and Nb(C,N) in the ferrite temperature region [18] and Thermo-Calc predicted stability below 680 ^{0}C. However, in the C-Nb-V steel the same annealing schedule resulted in dissolution of V-rich particles, which are predicted to be soluble in this steel above 500 ^{0}C, and precipitation of CuS (Figure 3,c,d and Figure 4), which was reported to form during annealing at 450 ^{0}C for 20 min [19] and at 500 ^{0}C for 5 min [20] in similar steel compositions. As it was difficult to separate any remaining V-rich and the CuS particles in the C-Nb-V annealed steel their average diameter and volume fraction were calculated together (Figure 5). Thus the average particle diameter at the mid-thickness position was measured to be 16.3 nm, particle volume fraction 0.00384 and particle number density 1426 μm^{-3}.

Dislocation sub-structure study

Thin foil TEM imaging revealed uniform dislocation density structures in both the C-Nb and C-Nb-V steels in the as-rolled and annealed conditions (Figure 6). Dislocation cell arrangements with regular space arrays were observed in both the steels. In the C-Nb-V steel numerous dislocation loop debris accompany the cell structure but in the C-Nb steel only a few loops were present. The cell size increases and the number of loops decreases after annealing (Figure 6,b,d). The dislocation density at the C-Nb steel plate mid-thickness position was measured to be in the range of 1.9 x 10^{14} m^{-2} to 3.1 x 10^{14} m^{-2} with an average value of 2.3 x 10^{14} m^{-2} for the as-rolled and 0.8 x 10^{14} m^{-2} to 2.0 x 10^{14} m^{-2} with an average value of 1.1 x 10^{14} m^{-2} for the annealed condition. In the C-Nb-V steel the dislocation density was in the range of 2.9 x 10^{14} m^{-2} to 5.2 x 10^{14} m^{-2} with an average value of 4.0 x 10^{14} m^{-2} for the as-rolled and 1.0 x 10^{14} m^{-2} to 2.8 x 10^{14} m^{-2} with an average value of 1.5 x 10^{14} m^{-2} for the annealed condition. Obtained data are in good agreement with the reported values for hot-rolled low carbon steels [21,22] and TMCR-processed X80 steel [3].

Reverse cold deformation

The Bauschinger effect during reverse cold deformation was studied using compression-tension testing stress-strain curves (Figure 7). The Bauschinger effect was assessed by the stress parameter according to the formula [23] (Figure 8):

$$\beta_\sigma = \frac{\sigma_p - \sigma_r}{\sigma_p} \qquad (1),$$

where σ_p is the maximum pre-stress and σ_r is the yield stress in the reverse direction taken at the point where the stress-strain curve deviates from the elastic deformation straight line (approximately 0.1% strain). As pre-strain and microalloying element content increase the stress parameter increases (Figure 8) [9,23,24]. Annealing led to the stress parameter decreasing with a larger relative drop for the C-Nb than for the C-Nb-V steel.

DISCUSSION

There are two principal Bauschinger effect theories (Figure 9); back stress and Orowan theory [13, 14]. During forward plastic deformation moving dislocations interact with different obstacles (other dislocations, grain boundaries, precipitates) preventing their further propagation. This generates a back stress around the contact point resisting further progress of similarly signed dislocations. During the

reverse deformation this back stress repels the dislocations from the obstacles in the opposite direction, namely in the direction of reverse strain. Thus the stress field helps to move the dislocations in the direction of reverse strain and the reverse yield stress drops by the level of the back stress. Materials with a larger number of dislocations (work-hardened after rolling) and obstacles (precipitates) would show a larger yield drop after reverse cold deformation due to the larger number density of dislocation-obstacle interaction sites. To predict the mechanical property change in practice one needs to correlate dislocation number density, particle number density (volume fraction and size) and the yield stress drop after deformation.

The influence of the back stress theory can be determined from the C-Nb steel since on annealing the dislocation density decreased by 1.2 x 10^{14} m^{-2}, whilst the particle size and number density remained constant, resulting in a Bauschinger stress parameter decrease of 0.08. On annealing the C-Nb-V plate material the dislocation density decreased by 2.5 x 10^{14} m^{-2}, which would suggest a larger (than 0.08) decrease in Bauschinger stress parameter, however, only a decrease of 0.02 – 0.04 (depending on the pre-strain) was observed. The change in precipitate population must, therefore, be associated with the deviation from expected behaviour. Annealing of the C-Nb-V steel resulted in the (partial) dissolution of the VC precipitates and formation of CuS particles with an increase in average diameter (16.3 nm compared to 6.3 nm) and decrease in number density (1426 μm^{-3} compared to 3873 μm^{-3}). The decrease in particle number density would be expected (by the Orowan theory) to cause a decrease in Bauschinger stress parameter, assuming that the particles interact with the dislocations in the same manner. However, an effective increase in Bauschinger stress parameter is observed which suggests that the very small VC particles are not effective obstacles to dislocations compared to the larger CuS precipitates so that even though the number density of particles decreases the number of 'effective' obstacles increases.

Comparing the C-Nb and C-Nb-V annealed plates there is a small increase in dislocation density (by 0.4 x 10^{14} m^{-2}) in the annealed C-Nb-V plate, which would suggest a small increase in Bauschinger stress parameter. However, the Bauschinger stress parameter increase is approximately 0.15, much greater than expected from the dislocation density change. This is caused by the significant difference in particle populations between the two plates, with an increase in number density in the annealed C-Nb-V steel due to the formation of the CuS precipitates, thus confirming the larger influence of these particles on the Bauschinger stress parameter.

Comparing the C-Nb and C-Nb-V as-rolled plates reveals an increase in dislocation density of 1.7 x 10^{14} m^{-2}, which would suggest an increase in Bauschinger stress parameter greater than 0.08 (seen for a change in dislocation density of 1.2 x 10^{14} m^{-2}). The measured change in Bauschinger stress parameter is approximately 0.07, close to that expected. There is a significant difference in particle populations between the two materials with the C-Nb-V steel having a greater number of large (>50 nm diameter) Nb(C,N) particles and a separate population of small (< 10 nm diameter) VC precipitates. The fact that this difference in precipitate population does not seem to have had any significant effect on the Bauschinger stress parameter difference between the steels also confirms the observation above that the CuS particles have the dominant influence. Further TEM study is required to investigate the dislocation – precipitate interactions more fully.

CONCLUSIONS

1. In the Nb- and Nb-V-alloyed steels the microalloying precipitate volume fraction increases from the sub-surface to the mid-thickness of the plates due to macro-segregation. Precipitate volume fraction and average size are larger in pearlite than in ferrite due to micro-segregation. Annealing of the Nb-

V-alloyed steel at 550^0C for 30 min resulted in V-rich particle dissolution and precipitation of CuS particles.

2. The TEM measured dislocation density at the C-Nb steel plate mid-thickness position was 2.3 x 10^{14} m^{-2} for as-rolled and 1.1 x 10^{14} m^{-2} for annealed condition; in the C-Nb-V steel – 4.0 x 10^{14} m^{-2} for as-rolled and 1.5 x 10^{14} m^{-2} for annealed condition. The obtained values correspond to literature data.
3. The Bauschinger stress parameter increases with an increase in dislocation density. Only the CuS particles (average diameter of 16.3 nm) had a significant effect on the Bauschinger stress parameter.

Acknowledgements

The authors would like to thank Corus UK Ltd. for provision of test material. Thanks are due to the Department of Metallurgy and Materials for the provision of research facilities at the University of Birmingham. One of the authors, (AK) is grateful to 'The Universities, UK' for awarding the scholarship to carry out his research in the UK.

REFERENCES

1. R.C. Ratnapuli and E.C. Rodrigues, Metals Technology, Vol. **9**, Nov., p. 440 – 445, 1982,
2. M. Graf and H.G. Hillenbrand, Production of large diameter line pipe – state of the art and future development trends, EUROPIPE, GmbH, www.europipe.de.
3. H.G. Hillenbrand, M. Graf and C. Kalwa, Development and production of high strength pipeline steels, EUROPIPE, GmbH, www.europipe.de, 2001.
4. H.G. Hillenbrand, C. Kalwa and A. Liessem, Technological solutions for ultra-high strength gas pipelines, EUROPIPE, GmbH, www.europipe.de, 2005.
5. H.G. Hillenbrand, A. Liessem, K. Biermann, C.J. Heckmann and V. Schwinn, Development of high strength material and pipe production technology for grade X120 line pipe, EUROPIPE, GmbH, www.europipe.de, 2004.
6. A. Streisselberger, J. Bauer, P. Flьss, H.G. Hillenbrand and P. Cordon, High strength steel plates for line pipes in grades up to X100, EUROPIPE, GmbH, www.europipe.de.
7. B. Hwang, S. Lee, Y.M. Kim, N.J. Kim and J.Y. Yoo, Metallurgical and Materials Transactions A, Vol. **36**, July, p. 1793 – 1805, 2005.
8. J. Bauer, P. Fless, E. Amoris and V. Schwinn, Ironmaking and Steelmaking, Vol. **32**, No 4, p. 325 – 330, 2005.
9. T.C. Harrison, R.T. Weiner and G.D. Fearnehough, Journal of Iron and Steel Institute, May, p. 334-336, 1972.
10. K. Nakajima, W. Mizutani, T. Kikuma and H. Matumoto, Transactions ISIJ, Vol. **15**, p. 1 – 10, 1975.
11. J.P. Ormandy, M. Strangwood and C.L. Davis, Material Science and Technology, Vol. **19**, May, p. 595 – 601, 2003.
12. K. Han, C.J. Van Tyne and B.S. Levy, Metallurgical and Materials Transactions, Vol. **36A**, Sept., p. 2379 – 2384, 2005.
13. P.S. Bate and D.V. Wilson, Acta Metallurgica, Vol. **34**, No. 6, p. 1097 – 1105, 1986.
14. L.M. Brown, Scripta Metallurgica, Vol. **11**, p. 127 – 131, 1977.
15. A.G. Kostryzhev, M. Strangwood and C.L. Davis, Materials Technology: Advanced Performance Materials, Vol. **22**, No. 3, p. 166 – 172, 2007.
16. D. Williams and C.B. Carter, Transmission electron microscopy, II – Diffraction, New York, Plenum Press, 1996.

17. C.L. Davis and M. Strangwood, Journal of Material Science, Vol. **37**, p. 1083–1090, 2002.
18. T. Gladman, The physical metallurgy of microalloyed steels, the Institute of Materials, Cambridge University Press, 1997.
19. I. Madariaga, J.L. Romero and I. Gutierrez, Metallurgical and Materials Transactions, Vol. **29A**, March., p. 1003 – 1015, 1998.
20. B. Garbarz, J. Marcisz and J. Wojtas, Material Chemistry and Physics, Vol. **81**, p. 486 – 489, 2003.
21. F. Yin, T. Hanamura, O. Umezawa and K. Nagai, Material Science and Engineering A, Vol. **354**, p. 31 – 39, 2003.
22. C.F. Robertson, K. Obrtlik and B. Marini, Journal of Nuclear Materials, Vol. **366**, p. 58 – 69, 2007.
23. A. Abel and H. Muir, Philosophical Magazine, Vol. **26**, p. 489 – 504, 1972.
24. D.N. Williams, Metallurgical Transactions A, Vol. **11**, Sept., p. 1629 – 1631, 1980.

TABLES

Table 1 Typical composition and mechanical properties of line-pipe steel plates

Steel grade	Typical composition, wt%	Process	Mechanical properties			Ref
			Yield,MPa	UTS,MPa	CVN*, J	
X60	0.12C-0.33Si-1.35Mn-0.04Nb-0.06V	TMCR	485	565		[1]
X65	0.08C-0.3Si-1.6Mn-0.08Nb-0.08V-0.017Ti-0.27Ni	TMCR	485-500	570-600	260 (-30^0C)	[2,3]
X70	0.09C-0.25Si-1.69Mn-0.05Nb-0.08V-0.003Ti-0.22Ni-0.01Mo	TMCR	500-580	600-790	200 (-10^0C)	[3]
X80	0.08C-0.4Si-1.9Mn-0.044Nb-0.019Ti-0.2Ni-0.01Mo-0.03Cr	TMCR + acc.cooling	600	730	180 (-20^0C)	[3]
X100	0.06C-0.33Si-1.95Mn-0.048Nb-0.019Ti-0.24Ni-0.3Mo	TMCR + acc.cooling	740-760	780-820	270 (-10^0C)	[4]
X120	0.05C-0.30Si-1.80Mn-0.80Cr-0.042Nb-0.017Ti-2.1Ni-0.70Mo	TMCR + acc.cooling	840-860	940-1130	260 (-30^0C)	[4,5]

* CVN - Charpy V-notch energy

Table 2 Plate composition in weight %

Steel grade	C	Si	Mn	P	S	Cr	Al	Ni	Cu	Nb	V	N	Ti	Mo
C-Nb	0.10	0.37	1.36	0.012	0.006	0.017	-	0.016	0.009	0.034	0.001	0.002	0.001	0.002
C-Nb-V	0.07	0.34	1.47	0.012	0.003	0.013	-	0.021	0.015	0.046	0.061	0.004	0.002	0.002

Table 3 Plate tensile properties (courtesy of Corus)

Steel grade	YS, MPa	UTS, MPa	Elongation to failure, %
C-Nb	487	568	21
C-Nb-V	557	590	19

Table 4 Microstructure characterisation

Steel grade	Grain size, μm		Pearlite content, %			Hardness HV
	sub-surface	mid-thickness	sub-surface	Mid-thickness	Thermo-Calc	
C-Nb	2.1 ± 0.2	3.0 ± 0.1	7.0 ± 0.6	11.6 ± 1.1	12.1	188 ± 16
C-Nb-V	1.9 ± 0.2	2.9 ± 0.1	3.1 ± 0.7	6.1 ± 0.8	6.5	194 ± 14

Table 5 Measurement results for the Nb-rich particles

area of precipitation		average diameter, nm				volume fraction				number density, μm^{-3}			
		C-Nb		**C-Nb-V**		**C-Nb**		**C-Nb-V**		**C-Nb**		**C-Nb-V**	
						f_{TC}* = 0.000365		f_{TC}^{*} = 0.001445					
sub-surface	ferrite	88	89	67	68	$4.4 \cdot 10^{-5}$	$6 \cdot 10^{-5}$	0.000372	0.000407	0.12	0.16	2.36	2.42
	pearlite	90		71		$9.7 \cdot 10^{-5}$		0.000476		0.25		2.54	
mid-thickness	ferrite	132	131	58	68	$6.7 \cdot 10^{-5}$	$5 \cdot 10^{-4}$	0.000165	0.000422	0.06	0.44	1.61	1.95
	pearlite	128		88		0.001325		0.000937		1.21		2.63	

*f_{TC} – particle volume fraction calculated with Thermo-Calc

FIGURES

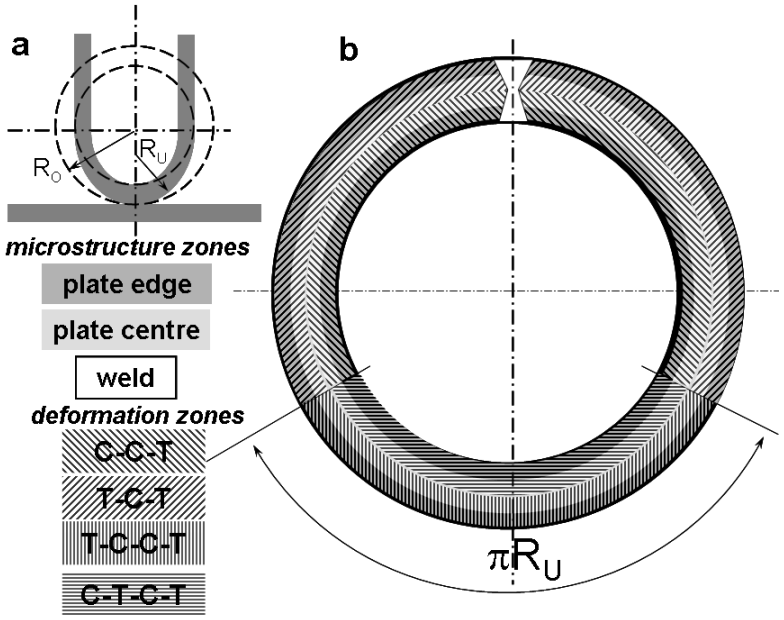

Figure 1 (a) Schematic diagram of the UOE forming process: R_U and R_O – outer radius of a pipe after U-ing and O-ing stages of forming; (b) Property zones in a pipe cross section after the UOE forming: C – compression, T – tension

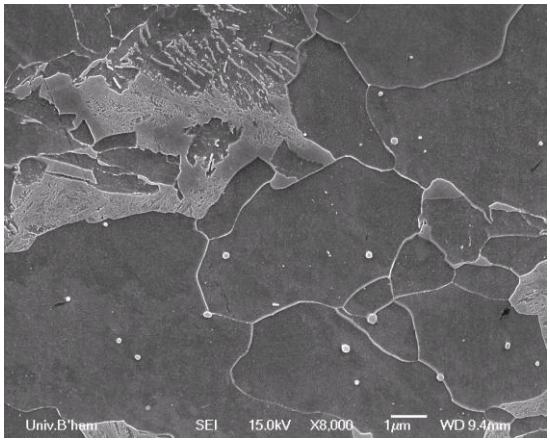

Figure 2 Typical SEM image from the C-Nb-V steel mid-thickness pearlite region

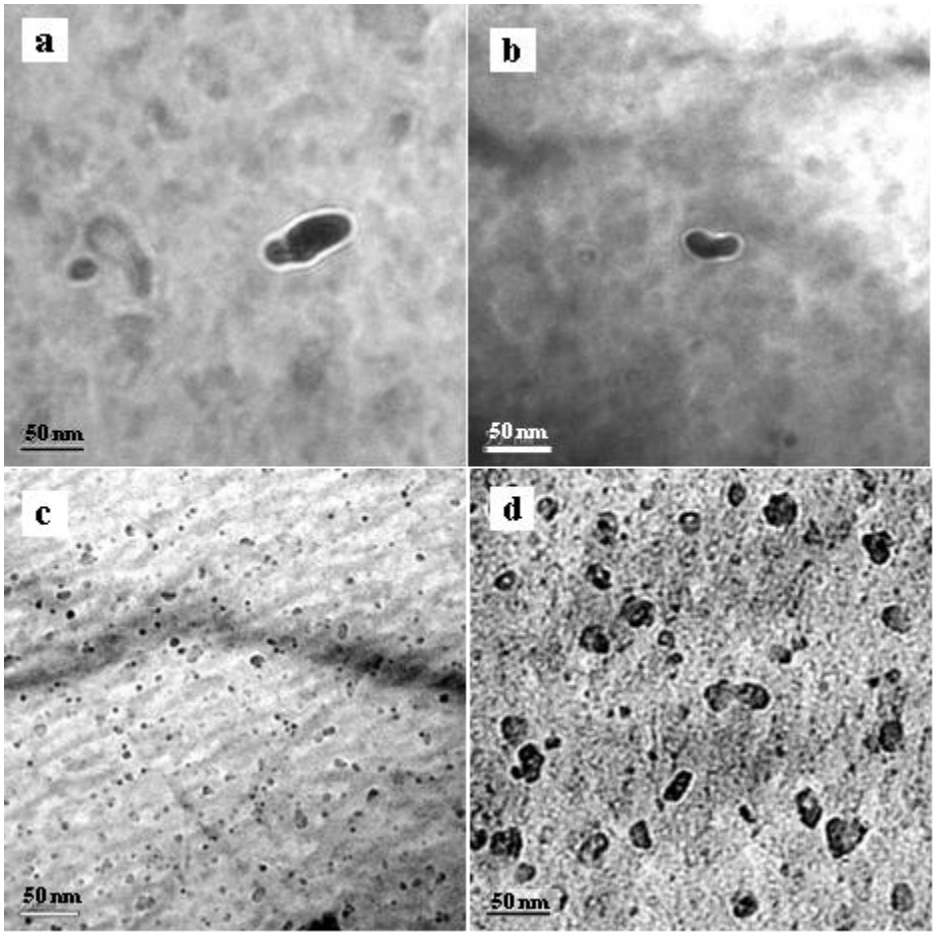

Figure 3 Selected TEM images of Nb-rich particles in the C-Nb (a) as-rolled and (b) annealed steel; typical TEM image of (c) V-rich particles in the C-Nb-V as-rolled and (d) V-rich + CuS in the C-Nb-V annealed steel

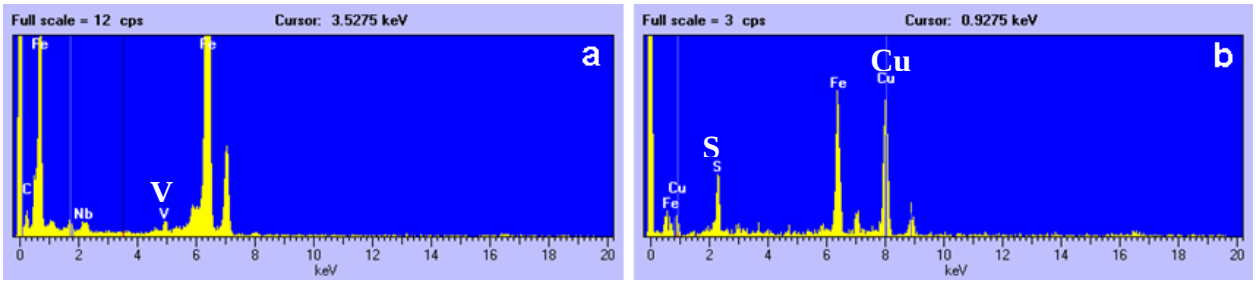

Figure 4 Typical EDS spectra of (a) V-rich and (b) CuS particles

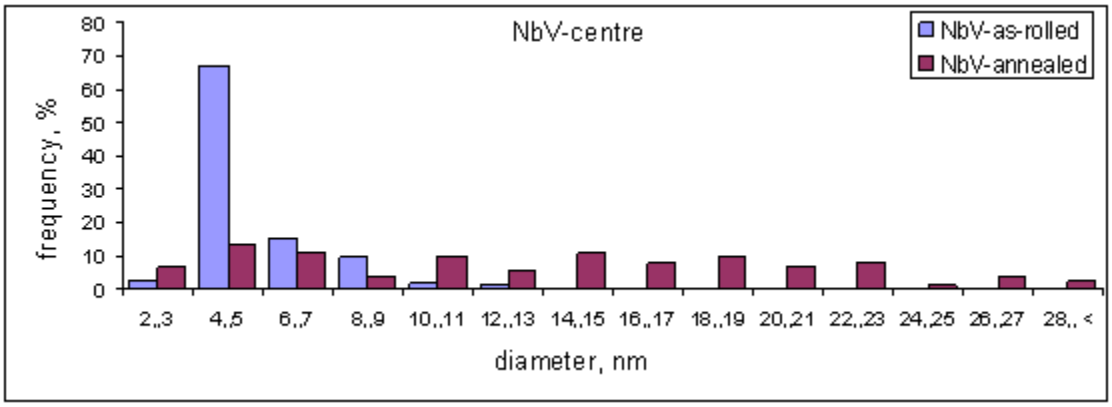

Figure 5 TEM measured particle distributions in the C-Nb-V as-rolled and annealed steel

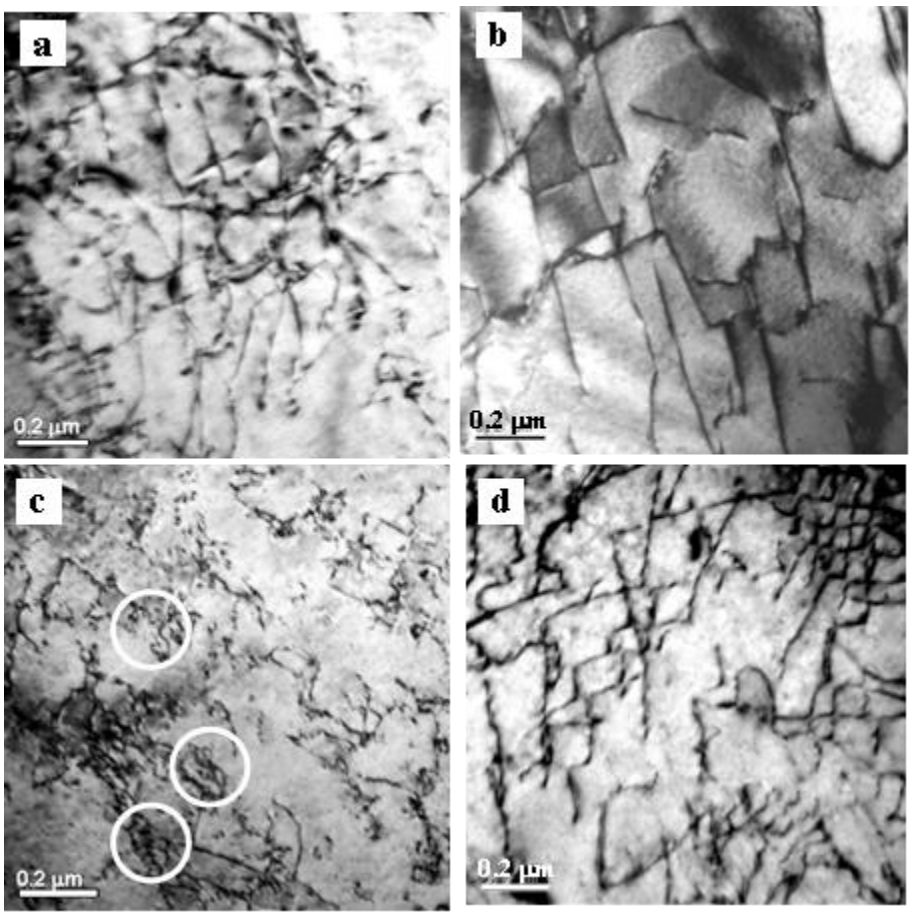

Figure 6 Typical TEM images of dislocation sub-structure in the C-Nb (a) as-rolled and (b) annealed; and C-Nb-V (c) as-rolled and (d) annealed steels: dislocation loops are shown with white circles

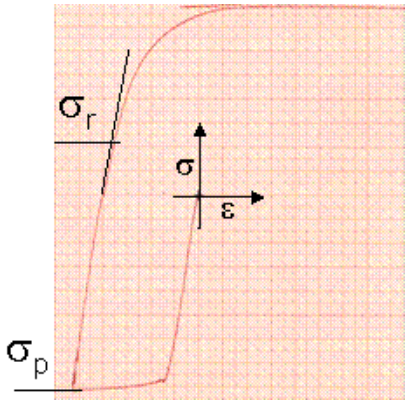

Figure 7 Typical stress-strain curve during compression-tension testing

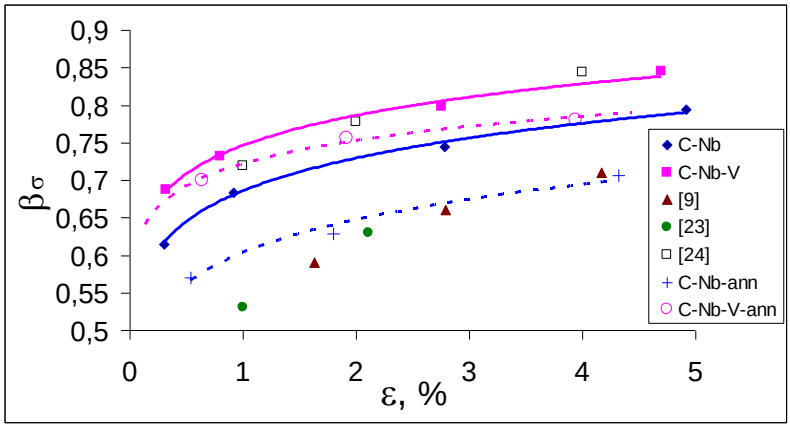

Figure 8 Bauschinger stress parameter versus pre-strain

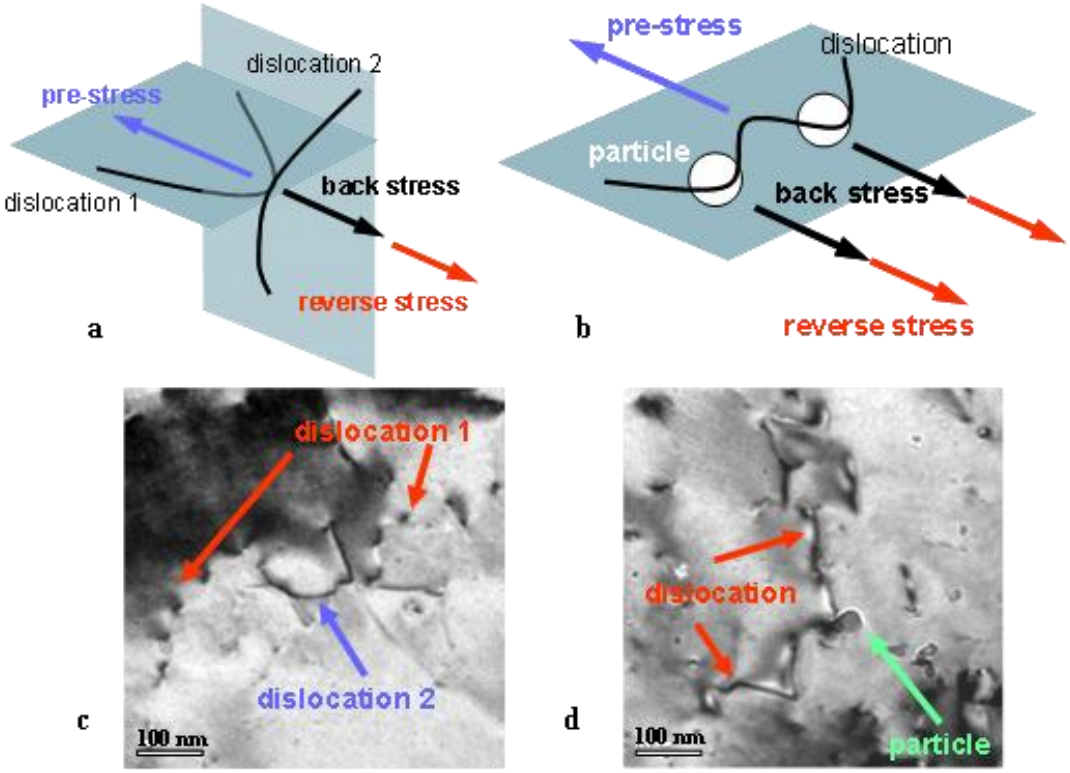

Figure 9 Schematic diagram and typical TEM micrograph of the dislocation-dislocation (a,c) and dislocation-particle (b,d) interaction